

AdaMorph: Unified Motion Retargeting via Embodiment-Aware Adaptive Transformers

Haoyu Zhang, Shibo Jin, Lvsong Li, Jun Li, Liang Lin, Xiaodong He, Zecui Zeng*

JD Explore Academy

Beijing, China

Abstract—Retargeting human motion to heterogeneous robots is a fundamental challenge in robotics, primarily due to the severe kinematic and dynamic discrepancies between varying embodiments. Existing solutions typically resort to training embodiment-specific models, which scales poorly and fails to exploit shared motion semantics. To address this, we present AdaMorph, a unified neural retargeting framework that enables a single model to adapt human motion to diverse robot morphologies. Our approach treats retargeting as a conditional generation task. We map human motion into a morphology-agnostic latent intent space and utilize a dual-purpose prompting mechanism to condition the generation. Instead of simple input concatenation, we leverage Adaptive Layer Normalization (AdaLN) to dynamically modulate the decoder’s feature space based on embodiment constraints. Furthermore, we enforce physical plausibility through a curriculum-based training objective that ensures orientation and trajectory consistency via integration. Experimental results on 12 distinct humanoid robots demonstrate that AdaMorph effectively unifies control across heterogeneous topologies, exhibiting strong zero-shot generalization to unseen complex motions while preserving the dynamic essence of the source behaviors.

I. INTRODUCTION

Data-driven motion retargeting has emerged as a critical technology for equipping robots with natural, human-like behaviors. By leveraging large-scale human motion datasets (e.g., AMASS [1]), robots can acquire diverse skills ranging from locomotion to gesturing. The goal is to establish a mapping function that translates a source human motion into a target robot trajectory while preserving the semantic intent.

However, this task is plagued by the *correspondence problem*: humans and robots possess distinct kinematic chains, joint limits, and mass distributions. Traditional pipelines largely rely on geometric Inverse Kinematics (IK) or optimization-based approaches [2, 3]. While physically accurate, these methods are computationally expensive, require meticulous manual tuning for each new robot, and often struggle with noisy input data. Recent learning-based approaches [4] offer a promising alternative but typically train separate, specialized networks for each embodiment. This one-robot-one-model paradigm ignores the shared semantic structure of motion and limits scalability.

We argue that a generalist retargeting system should decouple high-level *semantic intent* (e.g., “walking forward”) from low-level *morphological execution*. To this end, we introduce **AdaMorph**, a unified Transformer-based framework capable

of retargeting motion to heterogeneous robots using a single shared model.

Our approach diverges from standard methods in two key aspects. First, rather than simply appending robot descriptors to the input, we employ Adaptive Layer Normalization (AdaLN) [5]. We treat the robot embodiment as a style condition that globally modulates the normalization statistics of the motion decoder, effectively switching the generative dynamics to match the target kinematics. Second, to address the physical artifacts common in neural retargeting, we introduce a physics-compatible representation centered on base-frame velocities and enforce long-horizon consistency through differentiable integration and SO(3) projection.

In summary, our main contributions are as follows:

- We propose **AdaMorph**, a unified neural retargeting framework that decouples semantic intent from morphological execution, enabling a single policy to control heterogeneous robots.
- We introduce a **dual-pathway embodiment prompting** mechanism (combining token-level attention and layer-wise AdaLN modulation) to align shared motion intents with diverse robot kinematic manifolds.
- We design a **physics-constrained optimization** scheme that incorporates differentiable dead-reckoning, ensuring global trajectory consistency from local velocity predictions.
- We demonstrate that our unified model achieves **competitive performance** and robust motion tracking across multiple humanoid platforms without requiring embodiment-specific retraining.

II. RELATED WORK

A. Data-Driven Motion Retargeting

Translating motion between different morphologies is a classic problem in computer graphics and robotics. Optimization-based methods [2] minimize geometric energy functions to satisfy constraints but suffer from high computational costs. Learning-based methods treat retargeting as a supervised translation problem. approaches like [6, 7] utilize recurrent neural networks for skeleton-aware retargeting. However, most existing works focus on human-to-human or homogenous transfer. In robotics, methods typically train separate policies for each robot [8], limiting scalability. Our work

unifies this process, learning a single generator for multiple robotic agents.

B. Conditioning Mechanisms in Generation

To control generative models, various conditioning mechanisms have been proposed. Simple concatenation of condition tokens is widely used in language models. However, for continuous signal generation, feature-wise modulation often yields better results. Techniques like FiLM [9] and Adaptive Instance Normalization (AdaIN) [10] have demonstrated success in style transfer. Recently, Diffusion Transformers (DiT) [5] introduced AdaLN for class-conditional image generation. We adapt this insight to the motion domain, utilizing AdaLN to modulate motion features based on robot embodiment embeddings.

C. Physics-Compatible Motion Representation

Standard neural networks often output absolute positions, leading to global drift and physical inconsistencies. Phase-based representations [11] help synchronize cyclic motions but are complex to implement. Recently, MDME [12] demonstrated the efficacy of using local frame velocities and projected gravity for robust motion matching on legged robots. Building on this, we adopt a base-frame kinematic representation and further explicitly enforce physical consistency by integrating predicted velocities during training, penalizing deviations in the reconstructed global trajectory.

III. PRELIMINARIES

A. SMPL-Based Human Representation

We utilize the Skinned Multi-Person Linear (SMPL) model to represent human motion and morphology. The SMPL model is a vertex-based kinematic model parameterized by shape parameters β and pose parameters θ . In our framework, the shape parameters β play a crucial role in the *Dynamic Human Prompt* (Section IV), allowing the network to explicitly perceive the source subject's morphology (e.g., limb lengths and body proportions). The pose parameters θ , describing the relative rotation of body joints, serve as the source for articulation features.

B. Problem Formulation as Probabilistic Inference

We formulate unified motion retargeting as learning a conditional probability distribution over ground-truth robot motions $\mathbf{Y}^{(k)}$ given human demonstrations and embodiment descriptors. Let \mathcal{X}_h be the domain of human motions and $\{\mathcal{M}_r^{(k)}\}_{k=1}^K$ be the family of feasible kinematic manifolds for K distinct robot embodiments. The central challenge lies in mapping the human motion sequence \mathbf{X}_h to a robot-specific motion sequence $\hat{\mathbf{Y}}^{(k)}$, while strictly respecting the kinematic and dynamic constraints imposed by each robot's manifold $\mathcal{M}_r^{(k)}$. Mathematically, we seek to approximate the conditional distribution:

$$p_\theta(\mathbf{Y}^{(k)} \mid \mathbf{X}_h, \beta, k) \quad (1)$$

In practice, we predict the mean of an isotropic Gaussian distribution, reducing the maximum likelihood estimation (MLE)

to minimizing the ℓ_2 reconstruction distance. This formulation allows us to learn a shared latent intent space \mathcal{Z} that is invariant across the manifold family, while the decoding process projects this intent onto specific embodiment constraints.

C. Canonical Base-Frame Motion Representation

To facilitate cross-manifold transfer and eliminate global drift, we adopt a *canonical base-frame representation*. We define a local coordinate frame \mathcal{F}_t attached to the agent's root (pelvis for humans, trunk for robots). For any time step t , the root state comprises:

- **Local Linear Velocity (\mathbf{v}_t):** Computed via first-order finite differences in the world frame ($\mathbf{v}_t^{world} = (\mathbf{p}_t - \mathbf{p}_{t-1})/\Delta t$) and expressed in the base frame via $\mathbf{v}_t = \mathbf{R}_t^\top \mathbf{v}_t^{world}$. We use the root orientation $\mathbf{R}_t \in SO(3)$ at time t to ensure consistency with causal state estimation.
- **Local Angular Velocity (ω_t):** Derived from the relative rotation $\Delta \mathbf{R}_t = \mathbf{R}_{t-1}^\top \mathbf{R}_t$ via the logarithmic map: $\omega_t = \text{vee}(\log(\Delta \mathbf{R}_t))/\Delta t$, where $\text{vee}(\cdot)$ maps skew-symmetric matrices in $\mathfrak{so}(3)$ to axis-angle vectors.
- **Projected Gravity (\mathbf{g}_t):** The gravity vector $[0, 0, -1]^\top$ projected into the local base frame: $\mathbf{g}_t = \mathbf{R}_t^\top [0, 0, -1]^\top$. This feature is bounded by construction and kept unnormalized.

This representation disentangles local kinetics from global posture, serving as a shared interface for heterogeneous agents.

IV. METHODOLOGY

We introduce **AdaMorph**, a unified framework designed to disentangle semantic intent from morphological execution. As shown in Figure 1, AdaMorph employs a shared intent encoder, a dual-pathway embodiment-conditioned decoder, and embodiment-specific output adapters.

A. Input and Output Definition

Based on the canonical representation, we formally define the input and output spaces for the unified retargeting task.

1) *Human Input Sequence*: The input to the shared encoder, denoted as $\mathbf{X}_h \in \mathbb{R}^{T \times D_{in}}$, represents the human demonstration sequence derived from the SMPL model. For each time step t , the feature vector $\mathbf{x}_t^{(h)}$ is formulated as:

$$\mathbf{x}_t^{(h)} = [\mathbf{v}_t, \omega_t, \mathbf{g}_t, \mathbf{J}_t] \quad (2)$$

where $\mathbf{v}_t, \omega_t, \mathbf{g}_t \in \mathbb{R}^3$ denote the root linear velocity, angular velocity, and projected gravity in the canonical base frame. Crucially, $\mathbf{J}_t \in \mathbb{R}^{J \times 6}$ represents the local articulation. It is obtained by converting the SMPL pose parameters θ_t (excluding the global root orientation) into the 6D continuous rotation representation [13]. This transformation avoids the discontinuity issues associated with axis-angle or Euler angle representations while preserving the full kinematic information of the human subject.

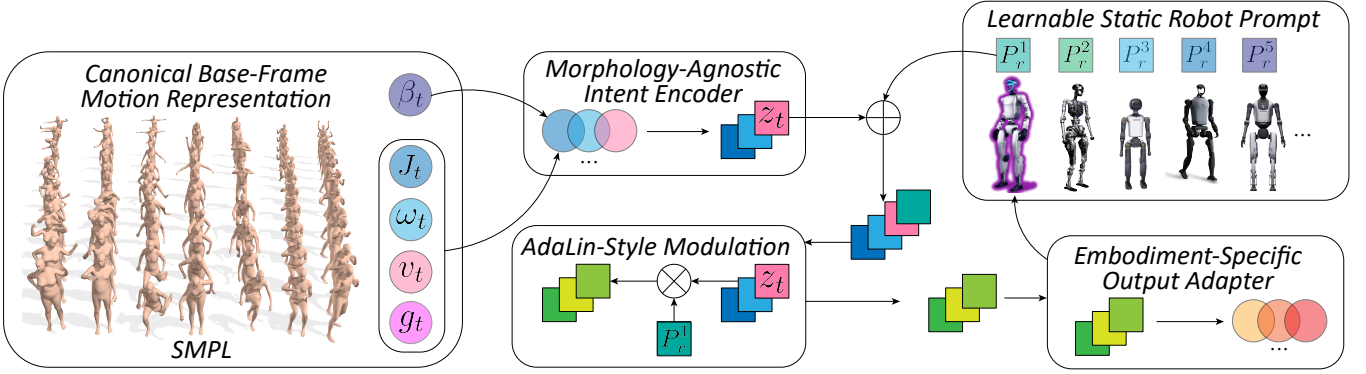


Fig. 1: Overview of the proposed **AdaMorph** framework. The architecture unifies cross-embodiment retargeting through a **Canonical Base-Frame Representation** that standardizes human motion features into local velocities and articulation (v_t, ω_t, g_t, J_t). (Left) A *Morphology-Agnostic Intent Encoder* maps these inputs, conditioned on SMPL shape parameters β via a Dynamic Human Prompt, to a shared latent intent z_t . (Right) To bridge kinematic disparities, **Learnable Static Robot Prompts** (P_r) drive the decoding process using *AdaLin-Style Modulation*, injecting embodiment-specific priors into the shared stream before **Embodiment-Specific Output Adapters** project the motion onto the target robot’s joint space.

2) *Robot Output Sequence*: The output for a specific robot k , denoted as $\hat{Y}_t^{(k)} \in \mathbb{R}^{T \times D_{out}^{(k)}}$, is generated by the embodiment-specific adapter. The predicted state vector $\hat{y}_t^{(k)}$ at time t explicitly disentangles the base dynamics from the articulation:

$$\hat{y}_t^{(k)} = [\hat{v}_t, \hat{\omega}_t, \hat{g}_t, \hat{q}_t] \quad (3)$$

- $\hat{v}_t, \hat{\omega}_t \in \mathbb{R}^3$: The predicted linear and angular velocities of the robot base, used for trajectory integration.
- $\hat{g}_t \in \mathbb{R}^3$: The predicted gravity vector, serving as a supervision signal for base orientation stability.
- $\hat{q}_t \in \mathbb{R}^{N_k}$: The joint positions (DoF) specific to the robot’s topology, where N_k is the number of controllable motors for robot k .

B. Dual-Pathway Embodiment Prompting

To bridge the gap between the shared intent and specific robot manifolds, we introduce a prompting mechanism that operates at two distinct structural scales.

Dynamic Human Prompt. An MLP adapter maps the SMPL shape parameters β to a sequence of soft tokens P_h , prefixing the encoder input to enable shape-aware intent extraction.

Static Robot Prompt. For each robot k , we learn a specific prompt bank $P_r^{(k)} \in \mathbb{R}^{L_p \times d_{model}}$. This prompt drives the decoding process through two complementary pathways:

1. *Token-Level Context via Cross-Attention*: The full prompt sequence acts as fine-grained memory. Within each decoder layer l , we compute cross-attention using the standard formulation:

$$\text{Attn}(\mathbf{Q}, \mathbf{K}, \mathbf{V}) = \text{softmax} \left(\frac{\mathbf{Q}\mathbf{K}^\top}{\sqrt{d_k}} \right) \mathbf{V} \quad (4)$$

where the query $\mathbf{Q} = \mathbf{H}_l \mathbf{W}_Q$ comes from the decoder hidden states, and keys/values are instantiated by the robot prompt: $\mathbf{K} = \mathbf{P}_r^{(k)} \mathbf{W}_K$, $\mathbf{V} = \mathbf{P}_r^{(k)} \mathbf{W}_V$. Here, d_k denotes the attention

head dimension. This mechanism allows the model to retrieve specific kinematic details from the prompt tokens.

2. *Layer-Wise Modulation via AdaLN*: We pool the prompt into a global vector $\mathbf{c}_{emb}^{(k)} = \text{Mean}(\mathbf{P}_r^{(k)})$ to drive Adaptive Layer Normalization (AdaLN). We regress **layer-specific** scale γ_l and shift \mathbf{b}_l parameters from $\mathbf{c}_{emb}^{(k)}$:

$$\text{AdaLN}_l(\mathbf{h}, \mathbf{c}_{emb}) = (1 + \gamma_l(\mathbf{c}_{emb})) \odot \text{LN}(\mathbf{h}) + \mathbf{b}_l(\mathbf{c}_{emb}) \quad (5)$$

where $\text{LN}(\cdot)$ is standard LayerNorm without affine parameters.

Zero-Initialization Property: We initialize the **last linear layer** of each modulation head to zero. Consequently, at the start of training, $\gamma_l \rightarrow 0$ and $\mathbf{b}_l \rightarrow 0$, reducing AdaLN to standard $\text{LN}(\mathbf{h})$. This ensures that optimization begins from a stable, shared decoder behavior before gradually specializing to distinct robot dynamics.

C. Morphology-Agnostic Intent Encoding

We employ a shared Transformer encoder to extract a morphology-agnostic intent representation. The input sequence concatenates the human prompt \mathbf{P}_h and projected motion features \mathbf{X}_h . The encoder yields a latent intent sequence $\mathbf{Z} \in \mathbb{R}^{T \times d_{model}}$. We explicitly discard the prompt portion of the output to ensure \mathbf{Z} represents the pure motion semantics rather than the conditioning context.

D. Embodiment-Specific Output Adapters

To resolve topology mismatch, we employ embodiment-specific MLP heads ψ_k . As defined in the output formulation, these heads project the shared latent representation \mathbf{z}_t to the robot-specific space \mathbb{R}^{9+N_k} . Mathematically, for robot k :

$$\hat{y}_t^{(k)} = \psi_k(\text{Dec}(\mathbf{z}_t, \mathbf{P}_r^{(k)})) \quad (6)$$

This architecture isolates the dimensional variance (N_k) within the lightweight final layers, preserving a unified parameter space for the heavy transformer backbone.

E. Physics-Constrained Optimization

Our training objective combines feature-space reconstruction with differentiable physical consistency constraints.

1) *Feature-Space Reconstruction*: We minimize the reconstruction error in the network’s standardized feature space:

$$\mathcal{L}_{inst} = \frac{1}{T} \sum_{t=1}^T \|\hat{\mathbf{y}}_t^{(k)} - \mathbf{y}_t^{(k)}\|_2^2 \quad (7)$$

2) *Differentiable Kinematic Consistency*: To enforce long-horizon validity, we model the trajectory reconstruction as a **discrete-time kinematic system**. We first recover the physical units from the network outputs (i.e., linear velocity $\hat{\mathbf{v}}_{phys}$ and angular velocity $\hat{\omega}_{phys}$). The global state evolves according to:

$$\hat{\mathbf{R}}_t = \hat{\mathbf{R}}_{t-1} \exp(\hat{\omega}_{phys,t} \Delta t) \quad (8)$$

$$\hat{\mathbf{p}}_t = \hat{\mathbf{p}}_{t-1} + \hat{\mathbf{R}}_t \hat{\mathbf{v}}_{phys,t} \Delta t \quad (9)$$

where $\hat{\mathbf{R}}_0$ and $\hat{\mathbf{p}}_0$ are initialized from ground truth during training.

Orientation Consistency. We minimize the geodesic distance on $SO(3)$ between the integrated state $\hat{\mathbf{R}}_t$ and the ground truth $\mathbf{R}_{gt,t}$ using a trace-based loss:

$$\mathcal{L}_{rot} = \frac{1}{T} \sum_{t=1}^T \left(1 - \frac{\text{Tr}(\hat{\mathbf{R}}_t^\top \mathbf{R}_{gt,t}) - 1}{2} \right) \quad (10)$$

To ensure geometric validity and prevent numerical drift, the integrated rotation matrices are projected back onto the $SO(3)$ manifold via Gram-Schmidt orthogonalization after each integration step.

Trajectory Consistency. We match the reconstructed displacement $\hat{\mathbf{d}}_t = \hat{\mathbf{p}}_t - \hat{\mathbf{p}}_0$ against the ground truth using a robust regression loss $\rho(\cdot)$:

$$\mathcal{L}_{traj} = \frac{1}{T} \sum_{t=1}^T \rho(\hat{\mathbf{d}}_t, \mathbf{p}_{gt,t} - \mathbf{p}_{gt,0}) \quad (11)$$

3) *Curriculum Learning Schedule*: Integrating predictions can lead to unstable gradients early in training. We employ a time-dependent weighting schedule:

$$\mathcal{L}_{total} = \mathcal{L}_{inst} + \lambda(s)(\mathcal{L}_{rot} + \mathcal{L}_{traj}) \quad (12)$$

where s is the global training step, and $\lambda(s)$ linearly warms up from 0 to λ_{max} . Additionally, we employ a Teacher Forcing strategy: we linearly decay the teacher-forcing ratio $\alpha(s)$ throughout training, progressively replacing the ground-truth orientation \mathbf{R}_{gt} with the integrated prediction $\hat{\mathbf{R}}$ in the velocity-rotation step.

V. EXPERIMENTS

To validate the effectiveness of our unified neural retargeting framework, we conducted extensive experiments on a large-scale dataset involving heterogeneous robot embodiments. We aim to answer three primary questions: (1) Can a single unified model effectively control diverse robot morphologies? (2) Does the model capture meaningful topological semantics

within its learned embodiment representations? (3) Does the framework generalize to out-of-distribution motion sequences?

A. Data Preparation and Preprocessing

1) *Dataset Construction*: We construct our training dataset based on the AMASS database [1], which provides a large-scale collection of high-quality human motion capture data. To obtain the corresponding ground-truth control signals for robotic agents, we leverage the state-of-the-art optimization-based method, *General Motion Retargeting* [14]. This method allows us to solve for physically feasible kinematic mappings from SMPL human parameters to robot joint spaces.

We initially considered a candidate pool of 16 distinct humanoid robot models. After a rigorous filtering process based on kinematic compatibility and solvability by the retargeting optimizer, we retained 12 robots for training and evaluation, excluding 4 models where physically valid kinematic solutions could not be reliably converged upon by the retargeting optimizer.

2) *Temporal Formatting and Augmentation*: To ensure the system meets the requirements of real-time control, we standardize the temporal resolution and window size of the data:

- **Downsampling**: The original human motion data, captured at 120Hz, is downsampled by a factor of 4 to match the standard control frequency of robotic platforms (30Hz).
- **Windowing**: We slice the continuous motion into short horizon segments. We empirically select a window size of $T = 60$ frames (approx. 2s). This horizon strikes a balance between capturing sufficient dynamic context for intent inference and maintaining low latency for real-time deployment.

The final processed dataset consists of approximately 30 million paired motion segments $(\mathbf{a}_h, \mathbf{a}_r)$, covering a wide range of locomotion and manipulation behaviors.

B. Implementation Details

Architecture Setup. The shared Transformer backbone is configured with $d_{model} = 768$, 12 layers, and 12 attention heads. The prompt length is set to $L_p = 16$.

Training Strategy. The model is trained for 200k steps using the AdamW optimizer ($lr = 5 \times 10^{-5}$) with a cosine schedule and a short linear warmup. We apply a dropout rate of 0.1. To mitigate gradient interference between heterogeneous embodiments, we employ a Round-Robin sampling strategy where each training step exclusively samples a batch from a single robot type.

Data Processing. All motion data is downsampled to 30Hz with a fixed past window size of $W = 60$. Velocities and DoF positions are standardized using dataset statistics; projected gravity and shape parameters are kept in their original scales.

C. Preliminary Results

We trained the model on the prepared 30M-sample dataset. We observed stable convergence of both the reconstruction and cross-modality losses, indicating that the shared latent space

Frame-by-Frame Comparison: Human Demonstration vs. Retargeted Robot Execution

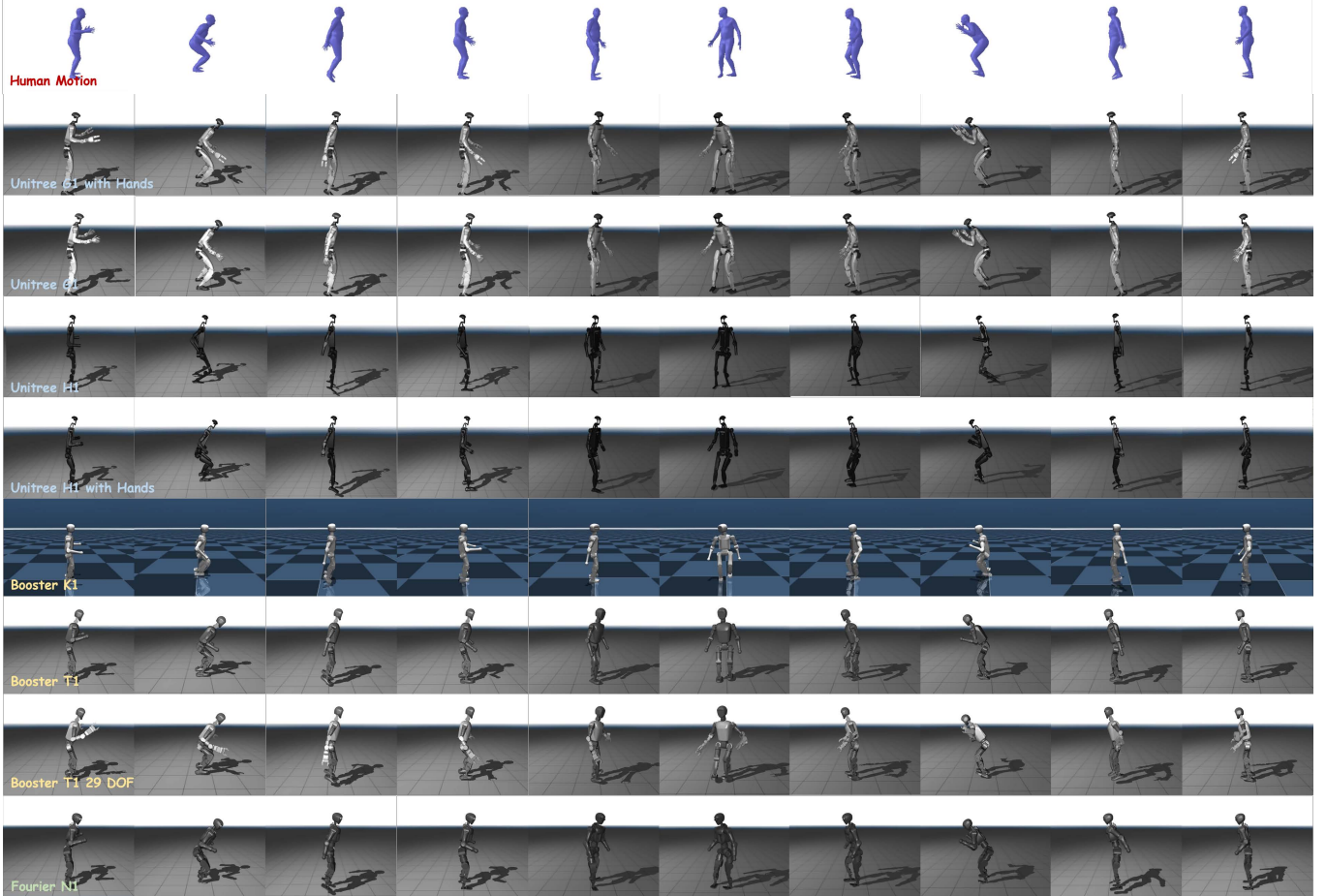


Fig. 2: **Qualitative validation in the MuJoCo physics simulator.** The unified model successfully retargets input human motions to all 12 trained robot embodiments. Despite the differences in link lengths and joint configurations, the robots faithfully reproduce the source behaviors, demonstrating the efficacy of our soft-prompted unified architecture.

is capable of aligning human kinematics with diverse robot morphologies.

To qualitatively validate the results, we visualized the generated motions in the MuJoCo physics simulator. As shown in Figure 2, the unified model successfully retargets input human motions to all 12 trained robot embodiments. Despite the differences in link lengths and joint configurations, the robots faithfully reproduce the source behaviors, demonstrating the efficacy of our soft-prompted unified architecture.

D. Analysis of Learned Robot Representations

Beyond qualitative retargeting performance, we investigated whether the proposed Soft-Prompted AdaLN architecture captures the underlying morphological semantics of different robots. We extracted the learnable robot prompt tokens from the trained model and conducted a comprehensive analysis of the learned latent space.

Topological Awareness in Latent Space. Figure 3(a) displays the cosine similarity matrix of the robot prompts. The matrix exhibits a clear block-diagonal structure, where

robots from the same series display significantly higher similarity scores compared to morphologically distinct robots. This indicates that the AdaLN module successfully learns to map similar kinematic constraints to proximal regions in the parameter space.

Semantic Clustering. The t-SNE visualization of the prompt tokens, shown in Figure 3(b), further reveals the semantic structure of the latent space. We observe two key properties:

- **Intra-Robot Consistency:** The 16 tokens for each robot form tight, well-separated clusters, confirming that the model learns a stable and unique “identity signature” for each embodiment.
- **Inter-Robot Semantics:** The relative distances between clusters reflect morphological affinities. For instance, the clusters for the Unitree G1 and Unitree H1 families are located in the same neighborhood, whereas the Booster and Fourier series form distant clusters.

These results demonstrate that our unified model does not simply memorize robot IDs but learns a structured, topology-

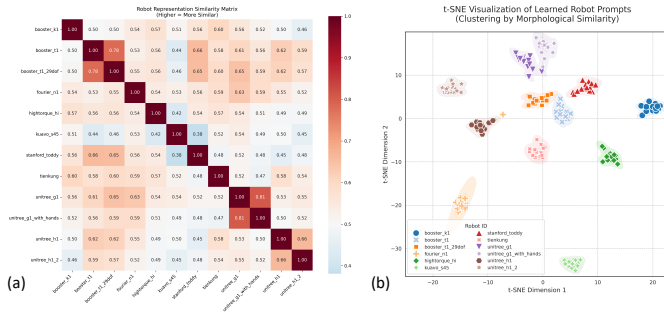


Fig. 3: Visualization of Learned Robot Representations.

(a) **Cosine Similarity Matrix:** The block-diagonal structure indicates high correlation between robots with similar kinematic chains (e.g., the Unitree family), proving that the model captures topological similarities. (b) **t-SNE Projection:** The projection of 16 learnable tokens per robot reveals semantic clustering. The model automatically groups robots by morphological similarity (e.g., G1 and H1 are proximal), forming stable identity signatures.

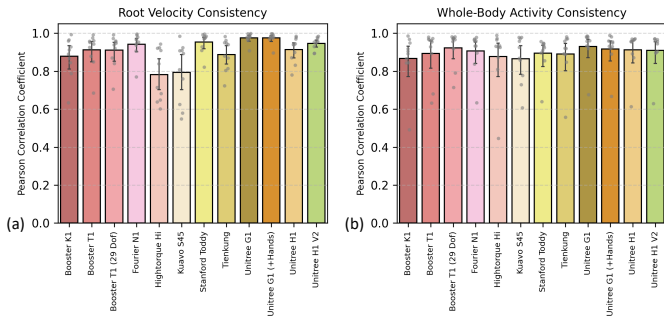


Fig. 4: Quantitative Evaluation of Semantic Consistency. (a) **Root Velocity Consistency:** The PCC between the root speed profiles of the human input and robot output. High correlations across diverse embodiments indicate that the robots accurately follow the human’s movement rhythm (e.g., acceleration and deceleration). (b) **Whole-Body Activity Consistency:** The PCC of the mean joint velocity magnitudes. The consistently high scores demonstrate that the model effectively transfers the overall energy and intensity of the motion, regardless of the robot’s specific kinematic configuration.

aware representation space that facilitates effective knowledge transfer across diverse embodiments.

E. Semantic Consistency and Activity Analysis

To strictly quantify the preservation of motion semantics during the retargeting process, we evaluated the rhythmic alignment between the source human motions and the generated robot behaviors. We employed the Pearson Correlation Coefficient (PCC) as the primary metric to assess temporal dynamics across two key dimensions: Root Velocity Consistency and Whole-Body Activity Consistency.

Rhythmic Alignment of Root Trajectories. Figure 4(a) presents the PCC results for root velocity consistency across

12 distinct robot embodiments. We observe that the model achieves high correlation scores across the board, with the Unitree G1 and H1 series exhibiting exceptional performance ($PCC \approx 0.95$). This indicates that despite significant differences in leg length and stride capacity, the robots faithfully replicate the temporal structure of the human locomotion, synchronizing their acceleration and deceleration phases with the source input. Even for morphologically distinct platforms like the Hightorque Hi and Kuavo S45, the median PCC remains above 0.8, confirming the robustness of our unified policy in preserving global movement intent.

Preservation of Motion Intensity. We further analyzed the Whole-Body Activity Consistency, defined as the correlation between the aggregate joint velocity magnitudes of the human and the robot. As shown in Figure 4(b), the model demonstrates remarkable consistency, with median PCC values exceeding 0.85 for all tested embodiments. Notably, the Booster T1 (29 DoF) and Unitree G1 achieve near-perfect correlation scores, suggesting that the “energy” of the motion, whether dynamic sprinting or subtle idling, is accurately translated into the robot’s joint space. These results substantiate that our Soft-Prompted AdaLN architecture goes beyond static pose matching to capture the dynamic essence of human motion.

F. Zero-Shot Generalization to Unseen Motion Domains

To assess the robustness of our learned representations, we evaluated the model’s performance on out-of-distribution motion sequences. We curated a specific hold-out test set consisting of distinct stylized ethnic dance performances (e.g., recordings from subjects such as *Stefanos Theodorou* and *Vaso Aristeidou*), which were strictly excluded from the training corpus. These sequences involve complex footwork, rapid directional changes, and rhythmic upper-body coordinations that differ significantly from the standard locomotion and manipulation tasks dominating the training distribution.

Despite the domain shift, our model successfully retargets these unseen dance motions to the target robots in a zero-shot manner. As illustrated in Figure 5, the robots faithfully replicate the artistic nuances and high-frequency dynamics of the source performance. This indicates that the shared intent encoder has learned a generalized understanding of human kinematics rather than merely memorizing specific training patterns. The ability to handle such distinct motion styles without fine-tuning further validates the efficacy of the proposed disentangled representation learning framework in capturing the underlying physics of motion.

VI. CONCLUSION

We have presented a unified neural retargeting framework that enables a single model to control heterogeneous robot embodiments. By mapping human motion into an *Implicit Intent* space and adapting it via *Soft Prompts*, our approach effectively decouples semantic intent from morphological constraints. Experiments across 12 distinct humanoids demonstrate that our method achieves high-fidelity, real-time motion

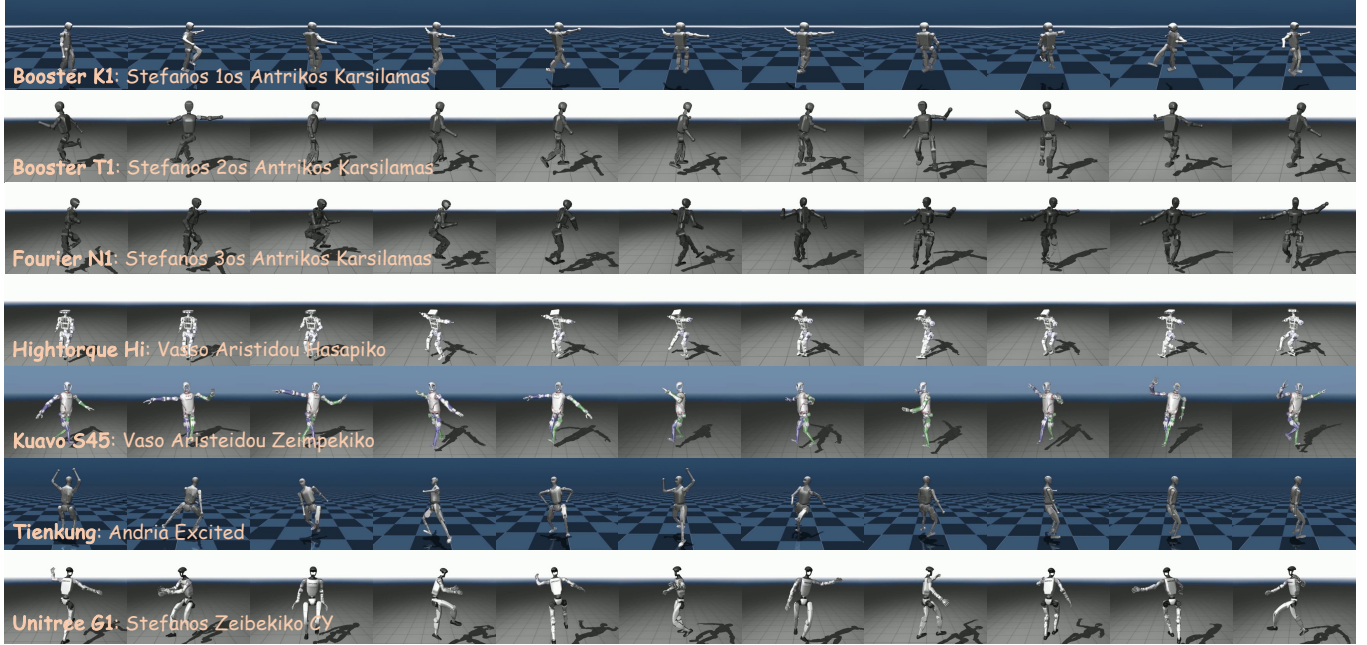


Fig. 5: **Zero-Shot Retargeting on Unseen Folk Dances.** Snapshots of diverse robots performing complex ethnic dance movements. Although these specific motion styles and subjects were completely absent from the training data, the unified model successfully transfers the intricate footwork and posture to the robot embodiments without any fine-tuning.

retargeting without the need for embodiment-specific training or offline optimization. Future work will focus on extending this framework to physics-based control for robust sim-to-real transfer.

ACKNOWLEDGMENTS

REFERENCES

- [1] N. Mahmood, N. Ghorbani, N. F. Troje, G. Pons-Moll, and M. J. Black, “Amass: Archive of motion capture as surface shapes,” in *Proceedings of the IEEE/CVF international conference on computer vision*, 2019, pp. 5442–5451.
- [2] M. Gleicher, “Retargetting motion to new characters,” in *Proceedings of the 25th annual conference on Computer graphics and interactive techniques*, 1998, pp. 33–42.
- [3] K. Ayusawa and E. Yoshida, “Motion retargeting for humanoid robots based on simultaneous morphing parameter identification and motion optimization,” *IEEE Transactions on Robotics*, vol. 33, no. 6, pp. 1343–1357, 2017.
- [4] A. Gupta, L. Fan, S. Ganguli, and L. Fei-Fei, “Metamorph: Learning universal controllers with transformers,” in *International Conference on Learning Representations*, 2022. [Online]. Available: https://openreview.net/forum?id=Opmqtk_GvYL
- [5] W. Peebles and S. Xie, “Scalable diffusion models with transformers,” in *Proceedings of the IEEE/CVF international conference on computer vision*, 2023, pp. 4195–4205.

- [6] R. Villegas, J. Yang, D. Ceylan, and H. Lee, “Neural kinematic networks for unsupervised motion retargeting,” in *Proceedings of the IEEE conference on computer vision and pattern recognition*, 2018, pp. 8639–8648.
- [7] K. Aberman, Y. Weng, D. Lischinski, D. Cohen-Or, and B. Chen, “Unpaired motion style transfer from video to animation,” *ACM Transactions On Graphics (TOG)*, vol. 39, no. 4, pp. 64–1, 2020.
- [8] X. B. Peng, P. Abbeel, S. Levine, and M. Van de Panne, “Deepmimic: Example-guided deep reinforcement learning of physics-based character skills,” *ACM Transactions On Graphics (TOG)*, vol. 37, no. 4, pp. 1–14, 2018.
- [9] E. Perez, F. Strub, H. De Vries, V. Dumoulin, and A. Courville, “Film: Visual reasoning with a general conditioning layer,” in *Proceedings of the AAAI conference on artificial intelligence*, vol. 32, no. 1, 2018.
- [10] X. Huang and S. Belongie, “Arbitrary style transfer in real-time with adaptive instance normalization,” in *Proceedings of the IEEE international conference on computer vision*, 2017, pp. 1501–1510.
- [11] S. Starke, I. Mason, and T. Komura, “Deepphase: Periodic autoencoders for learning motion phase manifolds,” *ACM Transactions on Graphics (ToG)*, vol. 41, no. 4, pp. 1–13, 2022.
- [12] M. Heyrman, C. Li, V. Klemm, D. Kang, S. Coros, and M. Hutter, “Multi-domain motion embedding: Expressive real-time mimicry for legged robots,” *arXiv preprint arXiv:2512.07673*, 2025.

- [13] Y. Zhou, C. Barnes, J. Lu, J. Yang, and H. Li, “On the continuity of rotation representations in neural networks,” in *Proceedings of the IEEE/CVF conference on computer vision and pattern recognition*, 2019, pp. 5745–5753.
- [14] J. P. Araujo, Y. Ze, P. Xu, J. Wu, and C. K. Liu, “Retargeting matters: General motion retargeting for humanoid motion tracking,” *arXiv preprint arXiv:2510.02252*, 2025.